Journal of Materials Chemistry C

PAPER

View Article Online
View Journal | View Issue

Cite this: J. Mater. Chem. C, 2014, 2, 946

A lanthanide-doping route to aspect-ratio-controlled KSc_2F_7 nanocrystals for upconversion, downconversion and magnetism†

Yujie Ding,[ab] Xiaoxia Zhang,[a] Hao Zhu[a] and Jun-Jie Zhu*[a]

Received 15th August 2013
Accepted 29th October 2013

DOI: 10.1039/c3tc31608d

www.rsc.org/MaterialsC

A novel route was developed by doping rare-earth ions (RE^{3+}) with large ionic radii (such as La^{3+}, Ce^{3+}, Sm^{3+}, Eu^{3+}, Tb^{3+}, Dy^{3+}, Yb^{3+} and Lu^{3+}) for aspect ratio modification of KSc_2F_7 nanocrystals (NCs). The results revealed that the shape of the nanocrystals could be readily tuned from one-dimensional long nanorods to zero-dimensional ultrasmall nanospheres. The aspect ratio of the NCs could be adjusted over a broad range from 45 to 1 by changing the dopant or doping concentration. Interestingly it was found that doping of a lanthanide with a larger ionic radius was equivalent to increasing the amount of the dopant on the aspect ratio evolution. The NCs doped with different RE^{3+} also exhibited multifunctionality, including upconversion (UC) and downconversion (DC) emissions as well as paramagnetic properties.

1. Introduction

The properties of NCs highly depend on their crystalline structure, size and shape, which raises an extraordinarily important challenge to synthesize NCs with desired morphology. Recently, a lot of NCs, such as oxides, fluorides and vanadates with precisely controlled dimensionality have been achieved *via* hydrothermal and thermodecomposition methods.[1–6] However, various parameters, including reaction temperature, time, monomer concentration and capping molecules, play an important role in the growth of the NCs. Thus, it is of fundamental importance to develop a readily controllable method for the preparation of these NCs with a desired size and simultaneously to modify their physical properties such as UC and DC emissions as well as magnetism.

Impurity doping, generally used to yield hybrid materials, by intentionally incorporating atoms or ions of suitable elements into host lattices, is one of the most effective routes to endow functional nanomaterials with magnetic and adjustable emission properties.[7] In fact, impurity doping was found to have a significant influence on the nucleation and growth of numerous NCs, thus providing a fundamental approach to alter the crystallographic phase, size, morphology, and electronic configuration of the nanomaterials. Very valuably, Wang and co-workers[8] reported the conversion of CeO_2 nanopolyhedra into nanospheres by Ti^{4+} doping, and Liu's group[9] demonstrated the rational tunability of the size and phase of $NaYF_4$ NCs by lanthanide doping. It was also found that lanthanide doping could modify the uneven size and shape of alkaline-earth fluoride NCs to monodisperse ultrasmall nanospheres,[10] and the introduction of Mg dopants could cause dramatic changes of the morphology of ZnO NCs.[11] Recently, some other useful impurity doping methods have been developed to control the shape of the nanomaterials.[12–14] These results suggested that impurity doping could greatly affect the growth of these nanoparticles and had been used as an effective way to yield NCs with proper size and shape. Unfortunately, simultaneously studying the effect of the size and amount of the dopant on controlling the morphology of NCs is rare. As a consequence, shape control of doped NCs is much less developed in comparison with that of undoped ones.

Lanthanide-based UC luminescent NCs show superior chemical and optical properties, including low toxicity, large anti-Stokes shifts, multicolor emissions, as well as high resistance to photobleaching, blinking, and photochemical degradation.[15–19] Hence, the controlled synthesis of lanthanide doped UC NCs has attracted a lot of interest and has been a popular topic for several decades.[20–28] Besides preparing general UC nanomaterials, we have proven that KSc_2F_7 nanorods are also excellent hosts giving a strong red UC luminescence when codoped with Yb^{3+}/Er^{3+}.[29] However, it may be difficult for the nanorods to be applied as bioprobes and for bioimaging because they are too long. Therefore, it is necessary to develop some novel methods for easy manipulation of the nucleation and growth kinetics of the KSc_2F_7 NCs leading to predictable morphology.

[a]State Key Laboratory of Analytical Chemistry for Life Science, School of Chemistry and Chemical Engineering, Nanjing University, Nanjing, 210093, China. E-mail: jjzhu@nju.edu.cn

[b]College of Biochemical Engineering, Anhui Polytechnic University, Wuhu, 241000, China

† Electronic supplementary information (ESI) available. See DOI: 10.1039/c3tc31608d

Herein we propose a lanthanide-doping route to synthesize KSc_2F_7 NCs with well-controlled aspect ratios. Generally, conventional synthetic techniques require stringent control over experimental parameters for tuning the crystalline structure, while the lanthanide-doping approach needs only a single variable, size or concentration of the dopants. Systematic studies on the impact of both the type and amount of dopants on aspect ratio evolution were conducted. This method can improve the ability to control the aspect ratio and bring about several important physical properties, such as UC and DC emissions and magnetism.

2. Experimental section

2.1. Materials

$RECl_3 \cdot 6H_2O$ (99.9%, RE = La, Ce, Sm, Eu, Tb, Dy, Yb, Lu, Ho, Gd and Sc), KOH (98%), NH_4F (98%), 1-octadecene (90%) and oleic acid (90%) were purchased from Sigma-Aldrich. All the materials were used directly without further purification. Deionized water was used throughout.

2.2. Characterization

Powder XRD measurement was performed on a Shimadzu XD-3A X-ray diffractometer at a scanning rate of $2° min^{-1}$ in the 2θ range from 10 to 80°, with graphite-monochromatized Cu-Kα radiation (λ = 0.15418 nm) and a nickel filter. FT-IR spectra were obtained on a Bruker Vector 22 spectrometer in the frequency range 4000–500 cm^{-1}. The morphology and microstructure were characterized by transmission electron microscopy (TEM) and high resolution TEM (HRTEM) using a JEOL-2100 TEM equipped with an Oxford Instrument energy-dispersive X-ray spectroscopy (EDS) system operating at 200 kV. The STEM studies were performed on a JEOL 2100F field emission electron microscope (equipped with an EDS system) with an acceleration voltage of 200 kV. The composition of the NCs was determined by an inductively coupled plasma mass spectrum (ICP-MS, Agilent Technologies 7500 series). X-ray photoelectron spectra (XPS) were measured on an ECSALAB 250. UC fluorescence spectra were recorded on a ZolixScan ZLX-UPL spectrometer using a continuous-wave laser (980 nm) as the excitation source with controllable power. DC fluorescence spectra were collected on a Shimadzu RF-5301 PC spectrofluorometer using a 150 W xenon lamp as the excitation source. The magnetization as a function of the applied magnetic field ranging from −80 to 80 kOe was measured using a Quantum Design PPMS-7 magnetometer at room temperature.

2.3. Synthesis

Synthesis of pure KSc_2F_7 NCs. The preparation of KSc_2F_7 NCs was developed *via* a modified literature procedure.[29] 1 mmol $ScCl_3 \cdot 6H_2O$ was added to a solution containing 15 mL oleic acid and 17.5 mL 1-octadecene. The system was heated to 160 °C for 30 min and then cooled down to room temperature. Thereafter, a 4 mL methanol solution containing NH_4F (1.6 mmol) and KOH (1.0 mmol) was added into the system, which was stirred for 30 min. After methanol was evaporated, the solution was heated to 300 °C under an argon atmosphere for 1 h. The resulting NCs were precipitated by the addition of ethanol, collected by centrifugation, washed with water and ethanol for several times.

Synthesis of KSc_2F_7: 10% RE^{3+} NCs (RE = Lu, Yb, Dy, Tb, Eu, Sm, Ce, La). The procedure for the synthesis of KSc_2F_7 NCs doped with 10% RE^{3+} was exactly the same as the preparation of the KSc_2F_7 NCs, except that 0.1 mmol $RECl_3 \cdot 6H_2O$ (RE = Lu, Yb, Dy, Tb, Eu, Sm, Ce and La, respectively) was added into the 50 mL three-necked flask at the same time. The total amount of $RECl_3 \cdot 6H_2O$ plus $ScCl_3 \cdot 6H_2O$ was 1 mmol for the preparation of each single sample.

Synthesis of KSc_2F_7: RE^{3+} NCs (RE = Sm, Eu, Tb, Dy; 1%, 5%, 20%). The procedure for the synthesis of KSc_2F_7 NCs doped with 1%, 5%, 20% RE^{3+} was exactly the same as the preparation of the KSc_2F_7 NCs, except that a fixed amount of $RECl_3 \cdot 6H_2O$ (RE = Sm, Eu, Tb, Dy, respectively) was added into the three-necked flask at the same time. The total amount of $RECl_3 \cdot 6H_2O$ and $ScCl_3 \cdot 6H_2O$ was a constant 1 mmol for the synthesis of every single sample.

Synthesis of KSc_2F_7: 10% Yb^{3+}, 1% Ho^{3+}, x% Gd^{3+} UC magnetic NCs (x = 0, 1, 5, 10, 15). The procedure for the synthesis of KSc_2F_7 NCs doped with 10% Yb^{3+}, 1% Ho^{3+} and x% Gd^{3+} (x = 0, 1, 5, 10, 15, respectively) was exactly the same as that used for the preparation of the KSc_2F_7 NCs, except that 0.1 mmol $YbCl_3 \cdot 6H_2O$, 0.01 mmol $HoCl_3 \cdot 6H_2O$ and a fixed amount of $GdCl_3 \cdot 6H_2O$ were added into a three-necked flask at the same time. The total amount of $ScCl_3 \cdot 6H_2O$, $YbCl_3 \cdot 6H_2O$, $HoCl_3 \cdot 6H_2O$ and $GdCl_3 \cdot 6H_2O$ was a constant 1 mmol for the synthesis of every single sample.

3. Results and discussion

The influence of the dopants on the aspect ratio evolution was investigated. The RE^{3+}-doped KSc_2F_7 NCs were synthesized with a reaction time of 1 h at a temperature of 300 °C when other experimental conditions remained unchanged.

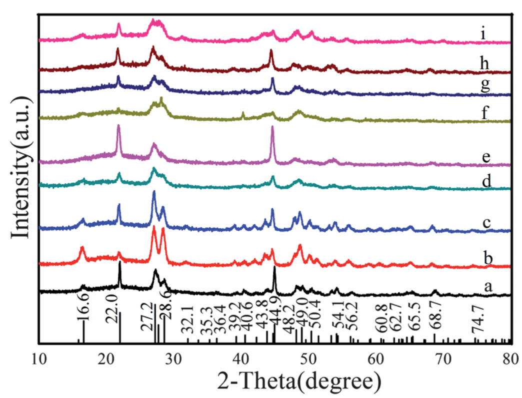

Fig. 1 XRD patterns of the KSc_2F_7 NCs. (a) Pure KSc_2F_7, (b) KSc_2F_7: 10% Lu^{3+}, (c) KSc_2F_7: 10% Yb^{3+}, (d) KSc_2F_7: 10% Dy^{3+}, (e) KSc_2F_7: 10% Tb^{3+}, (f) KSc_2F_7: 10% Eu^{3+}, (g) KSc_2F_7: 10% Sm^{3+}, (h) KSc_2F_7: 10% Ce^{3+}, (i) KSc_2F_7: 10% La^{3+} and line pattern (lower part) of the orthorhombic phase KSc_2F_7 (JCPDS card 77-1321).

Fig. 1 displays the XRD patterns of the pure and 10% RE^{3+} (RE = Lu, Yb, Dy, Tb, Eu, Sm, Ce, La) doped KSc_2F_7 NCs, respectively. The samples are at high crystallinity and all the peak positions match well with the end-centered orthorhombic structure of the KSc_2F_7 NCs, whose cell parameters are $a = 1.064$ nm, $b = 0.654$ nm, and $c = 0.403$ nm. The diffraction peaks have slight changes in the relative intensity compared to those of standard data, implying the existence of a preferential orientation for the NCs.[30] An apparent shift towards small values can be observed for 2-theta due to the doping of RE^{3+} with a larger ionic radius ($r = 0.085$–0.106 nm) compared to that of Sc^{3+} ($r = 0.0745$ nm).[31,32] What is more, with the ionic radius of the dopants increasing, the diffraction peaks with an enlarging breadth appear. Therefore, larger-sized dopants are preferred to form smaller NCs.

The presence of oleic acid on the NCs' surface was confirmed by the FT-IR spectrum (Fig. S1†). Because of the existence of the capping ligand, the NCs could be dispersed into nonpolar solvents, *e.g.*, cyclohexane, toluene, and so on, for several weeks without settling. For some representative samples, the incorporation of RE^{3+} ions into the KSc_2F_7 NCs was confirmed by EDS (Fig. S2†). The element mapping of an individual nanorod from the STEM is presented in Fig. S3.† For the KSc_2F_7: 10% Yb^{3+} nanorod shown here, strong K and Sc signals are discovered in the same region as the intense F signals, indicating the existence of the KSc_2F_7 hosts. There is only a small amount of Yb contained in the nanorod, as indicated by the very low level of signal for the Yb map, which agrees well with the low doping content of Yb. The content of the doped RE^{3+} ions was calculated based on the cationic precursors (actual doping content achieved by ICP-MS is shown in Table S1†).

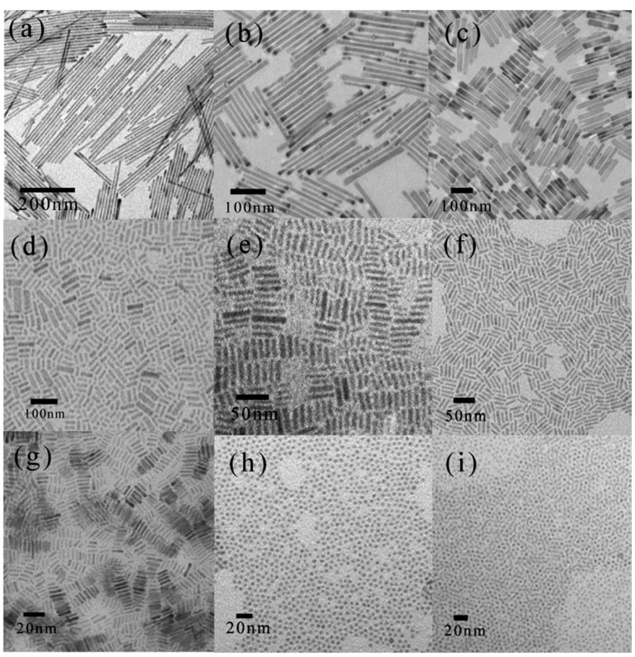

Fig. 2 TEM images of (a) pure KSc_2F_7 NCs, and (b) 10% Lu^{3+}, (c) 10% Yb^{3+}, (d) 10% Dy^{3+}, (e) 10% Tb^{3+}, (f) 10% Eu^{3+}, (g) 10% Sm^{3+}, (h) 10% Ce^{3+}, (i) 10% La^{3+} doped KSc_2F_7 NCs, respectively.

The TEM images of undoped KSc_2F_7 NCs and the resulting NCs doped with 10% RE^{3+} (RE = Lu, Yb, Dy, Tb, Eu, Sm, Ce, La, respectively), are shown in Fig. 2. According to the TEM results, Table 1 shows the doping effect of the RE^{3+} on the length, diameter and aspect ratio of the KSc_2F_7 NCs. The undoped NCs were measured to be big nanorods with 223 nm length and 5 nm width, resulting in an aspect ratio of 45. However, after lanthanide doping, the size and shape of the KSc_2F_7 NCs changed remarkably. More specifically, with the alteration of the lanthanide dopants from Lu^{3+} to La^{3+}, the ionic radius increased from 0.085 nm (Lu^{3+}) to 0.106 nm (La^{3+}). Correspondingly, the shape of the KSc_2F_7 NCs changed from long nanorods, to short nanorods, and finally to ultrasmall nanospheres with lengths of 161, 118, 57, 35, 29, 12, 5 and 4 nm, respectively. Nevertheless, the diameter changes were over a relatively small range, so the aspect ratio could be slowly tuned from 45 to 1. For the KSc_2F_7 NCs doped with 10% Ce^{3+} or 10% La^{3+}, as shown in the histograms (Fig. S4a and b†), the nanoparticles have a homogeneous morphology with a very narrow size distribution. These results confirmed that dopants with a larger ionic radius could decelerate the anisotropic crystalline growth and help to form small NCs with decreased aspect ratios, while smaller-sized dopants had a tiny influence on the aspect ratio evolution of the NCs.

The crystalline nature of the KSc_2F_7 NCs undoped or doped with 10% Yb^{3+}, 10% Sm^{3+} and 10% Ce^{3+}, respectively, was revealed by HRTEM (Fig. 3a–d). The lattice arrangements of the atoms in all the NCs can be clearly observed, showing the single crystallinity of the KSc_2F_7 samples. This correlates well with their SAED patterns as shown in the insets of Fig. 3.

At the same time, fixing Sm^{3+} as the dopant, KSc_2F_7 NCs with different doping concentrations (1%, 5%, 10%, 20%) were compared. The XRD patterns (Fig. 4) match well with those of standard orthorhombic structured KSc_2F_7 (JCPDS card 77-1321), and no peaks from other phases or impurities are observed. Some diffraction peaks can not be observed compared to standard data because of a preferential orientation for the nanorods.[31] Peaks with bigger widths emerge with increased Sm^{3+} concentrations, suggesting that smaller NCs are formed.

Fig. 5 shows the TEM images of the KSc_2F_7 NCs doped with 1%, 5%, 10%, 20% Sm^{3+}, respectively. The lengths, diameters and aspect ratios are listed in Table 2. NCs of gradually

Table 1 Length, diameter and aspect ratio from the TEM pictures in Fig. 2

Dopants (10%)	Length (nm)	Diameter (nm)	Aspect ratio
No doping	223	5	45
Lu^{3+}	161	9	18
Yb^{3+}	118	17	7
Dy^{3+}	57	12	5
Tb^{3+}	35	7	5
Eu^{3+}	29	7	4
Sm^{3+}	12	3	4
Ce^{3+}	5	5	1
La^{3+}	4	4	1

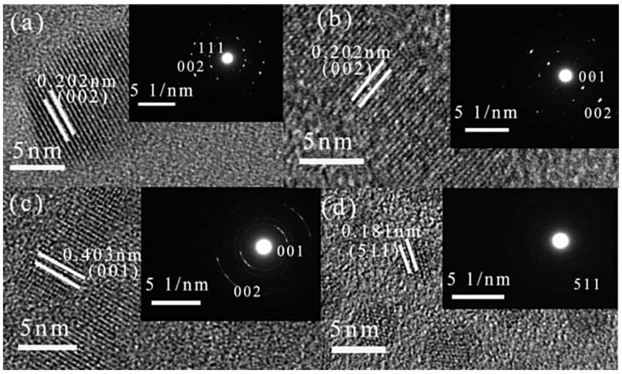

Fig. 3 HRTEM of (a) pure KSc_2F_7, (b) KSc_2F_7: 10% Yb^{3+}, (c) KSc_2F_7: 10% Sm^{3+}, (d) KSc_2F_7: 10% Ce^{3+}. Insets of (a–d) are the selected-area electron diffraction (SAED) patterns of the corresponding HRTEM images.

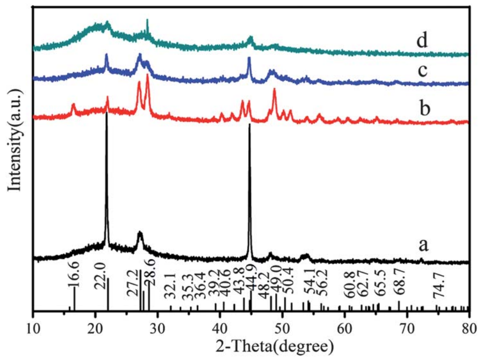

Fig. 4 XRD patterns of the KSc_2F_7 NCs. (a) KSc_2F_7: 1% Sm^{3+}, (b) KSc_2F_7: 5% Sm^{3+}, (c) KSc_2F_7: 10% Sm^{3+}, (d) KSc_2F_7: 20% Sm^{3+} and a line pattern (lower part) of the orthorhombic phase KSc_2F_7 (JCPDS card 77-1321).

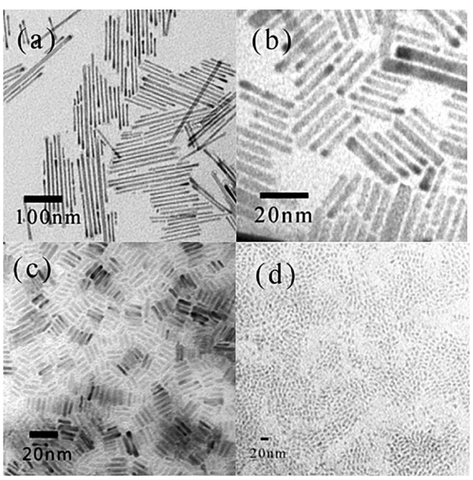

Fig. 5 (a–d) TEM images of the resulting KSc_2F_7 NCs doped with 1%, 5%, 10%, 20% Sm^{3+}, respectively.

decreasing aspect ratios were formed with an increase in the amount of Sm^{3+}. Interestingly, in the presence of 20% Sm^{3+}, the products became ultrasmall nanospheres with a uniform diameter of 3 nm, which shared the same aspect ratio as 10%

Table 2 Length, diameter and aspect ratio from the TEM images in Fig. 5

Concentration (Sm^{3+})	Length (nm)	Diameter (nm)	Aspect ratio
1%	110	8	14
5%	21	3	7
10%	12	3	4
20%	3	3	1

La^{3+} or 10% Ce^{3+} doped NCs. A histogram of the size distribution of the 20% Sm^{3+} doped KSc_2F_7 nanospheres is shown in Fig. S4c.†

The graph of the aspect ratio *versus* length for 10% RE^{3+} and x% Sm^{3+} ($x = 0, 1, 5, 10, 20$) doped KSc_2F_7 NCs is drawn in Fig. 6. The aspect ratio reduced with increasing Sm^{3+} content, similar to the case of doping with larger-sized lanthanides. Hence, doping of a lanthanide with a larger ionic radius is equivalent to increasing the amount of the dopant on the aspect ratio evolution. Therefore, this approach can control aspect ratio *via* doping RE^{3+} with different ionic radii or concentrations.

For the lanthanide doped KSc_2F_7 NCs, the RE^{3+} is likely to substitute Sc^{3+} rather than K^+ in the occupation site, because (1) the ionic radius of Sc^{3+} is 0.0745 nm, a little smaller than that of the other RE^{3+} dopants (between 0.085 and 0.106 nm), and much smaller than that of 0.138 nm for K^+; (2) Pauling's electronegativity of Sc^{3+} is 1.42, much closer to that of the other RE^{3+} (between 1.33 and 1.48), but much larger than the value of 0.99 for K^+; and (3) there exists a huge charge difference between Sc^{3+} and K^+.[33] For homo-valence ion doping, the crystalline lattice can contract or expand when small- or large-sized impurities are doped to substitute the host ions. One part of RE^{3+} was homogeneously incorporated into the KSc_2F_7 host lattice, bringing about a monotonous lattice expansion, which could certainly increase the nucleation energy and inhibit heterogeneous nucleation. Inevitably, it might be responsible for the monotonous decrease in the size.[7] The other part of the RE^{3+} might be expelled from the internal bulk lattice to the surface by a "self-purification" process.[34] Thus, a large number of the RE^{3+} ions were expected to

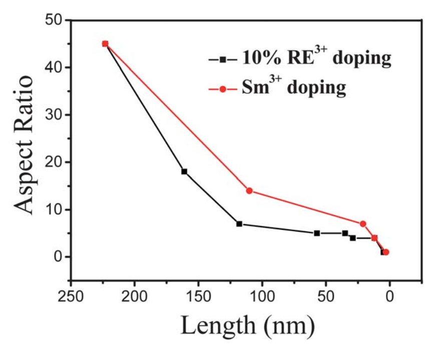

Fig. 6 Graph of aspect ratio *versus* length for 10% RE^{3+}-doped KSc_2F_7 NCs (the black dots from left to right are no doping, Lu^{3+}, Yb^{3+}, Dy^{3+}, Tb^{3+}, Eu^{3+}, Sm^{3+}, Ce^{3+} and La^{3+} doping, respectively) and Sm^{3+}-doped KSc_2F_7 NCs (the red dots from left to right are 0%, 1%, 5%, 10% and 20% doping, respectively).

occupy the surface sites of the KSc_2F_7 NCs, resulting in the rearrangement of the nearest-neighbor ions, and therefore decreasing the crystallinity and prohibiting the coalescence of tiny KSc_2F_7 single crystals to larger sizes.[33,35,36] As a consequence, dopants of higher concentrations or larger ionic radii can affect the size and aspect ratio evolution more significantly.

XPS was carried out to identify the chemical composition and the valence state of the elements. Fig. 7 shows the XPS survey spectra of pure and Sm^{3+} doped KSc_2F_7 NCs (Fig. 7a) as well as the Sm 3d spectrum (Fig. 7b). The peaks can be ascribed to K, Sc, F, C and O elements for pure and Sm, K, Sc, F, C and O for Sm^{3+}-doped KSc_2F_7 NCs, respectively. The core level Sm $3d_{3/2}$ and Sm $3d_{5/2}$ peaks are observed at binding energies of 1110.2 and 1082.9 eV, respectively, confirming that Sm exists as a chemical state of Sm^{3+} within the KSc_2F_7 NCs. The XPS analysis clearly verifies the doping of Sm and successive formation of Sm^{3+}-doped KSc_2F_7 NCs as expected.

To further test the accuracy of the proposed conclusion, we extended our experiment to other related systems. With the same method, Eu^{3+}, Tb^{3+} and Dy^{3+} (1%, 5%, 10%, 20%)-doped KSc_2F_7 NCs were prepared, respectively. The XRD patterns of the samples (Fig. S5†) agree well with the standard orthorhombic structure of KSc_2F_7 NCs (JCPDS card 77-1321). The growth of the NCs was also modified by these dopants, similar to Sm^{3+}-doped NCs, as evidenced in Fig. S6, Table S2 and Fig. S7.† Because of the smaller-sized dopants, the 20% Tb^{3+} or 20% Dy^{3+}-doped NCs turned out to be short nanorods instead of ultrasmall nanospheres. It was predicted that increasing of the doping concentration could also achieve NCs with an aspect ratio of 1.

Doping of impurity ions into the NCs can not only alter the length and aspect ratios but also lead to excellent properties. The KSc_2F_7 NCs show favourable multifunctionality through similar lanthanide-doping routes.

Under 980 nm excitation, as shown in spectrum a of Fig. 8A, the Yb^{3+}–Ho^{3+} codoped KSc_2F_7 NCs emit dominant green UC luminescence ascribed to $^5F_4$–$^5I_8$ of Ho^{3+}. With the increase of the Gd^{3+} doping amounts (1%, 5%, 10%, 15%), the green light becomes weak. Because of Gd^{3+} doping, the crystalline size decreases significantly, which can increase surface quenching sites, subsequently weakening the UC emission efficiency.[37,38] When the doping concentration of Gd^{3+} becomes 15%, the observed UC emission composed of a yellow and purple color appears, because the purple (409 nm) to green (539 nm) ratio is enhanced with an increase of the Gd^{3+} doping content. The reason may be that when Gd^{3+} ions are doped into the KSc_2F_7 hosts, the crystalline lattice will be slightly expanded, and the distance between sensitizer ions (Yb^{3+}) and activator ones (Ho^{3+}) is enlarged. Thus, the energy transfer from Yb^{3+} to Ho^{3+} will be influenced, eventually leading to a change of the UC colors. The insets of Fig. 8A display photographs of the eye-visible luminescence from the corresponding NCs. As illustrated above, the emission colors can be readily tuned from bright green to yellow and finally to purple *via* modifying the Gd^{3+} doping content. Fig. S8 and S9† depict the details of power dependence and energy transfer mechanism of the UC emission, respectively.

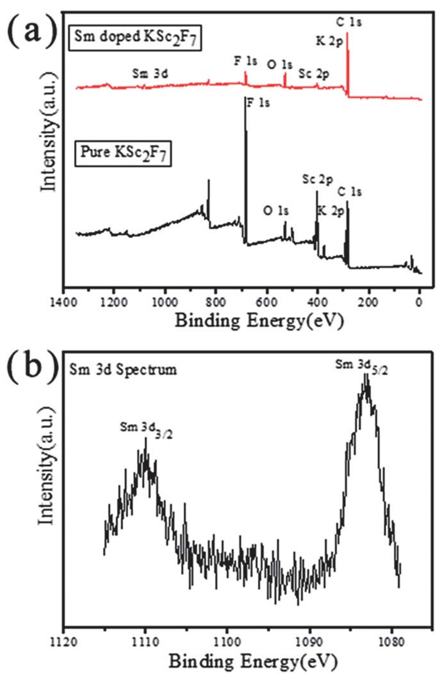

Fig. 7 (a) XPS survey spectra of pure KSc_2F_7 and 20% Sm^{3+} doped KSc_2F_7 NCs. (b) The Sm 3d spectrum.

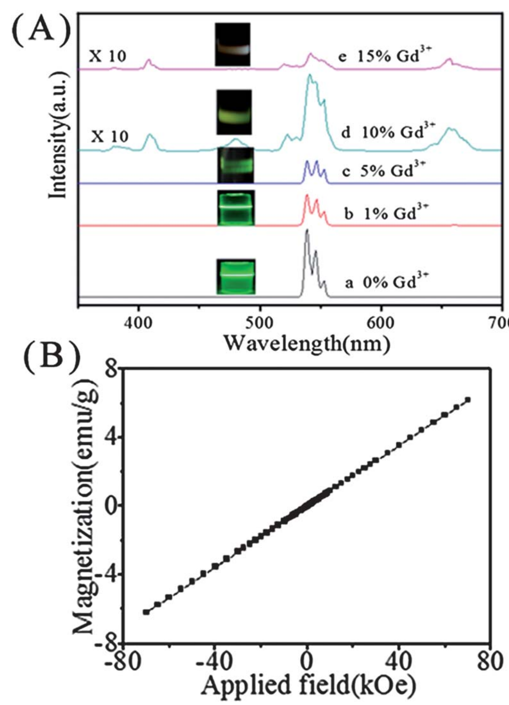

Fig. 8 (A) UC luminescence spectra of KSc_2F_7: 10% Yb^{3+}, 1% Ho^{3+}, x% Gd^{3+} NCs. (a) 0% Gd^{3+}, (b) 1% Gd^{3+}, (c) 5% Gd^{3+}, (d) 10% Gd^{3+}, (e) 15% Gd^{3+}. UC luminescence intensity of the (d) and (e) were magnified 10 times for the sake of comparison. Insets are the UC luminescence photography of the corresponding materials. The photographs were taken from 1 wt% cyclohexane solution under 980 nm excitation. (B) Magnetization as a function of applied field for KSc_2F_7: 10% Yb^{3+}, 1% Ho^{3+}, 15% Gd^{3+} NCs.

Besides the UC emission, the Yb^{3+}–Ho^{3+}–Gd^{3+} codoped KSc_2F_7 NCs also exhibit paramagnetism at room temperature, which is generated from the intrinsic magnetic moment of Gd^{3+} ions with non-interacting and localized nature. Fig. 8B shows the magnetization as a function of applied magnetic field (from −80 to 80 kOe) of the KSc_2F_7 NCs doped with 10% Yb^{3+}, 1% Ho^{3+} and 15% Gd^{3+}. The magnetic mass susceptibility is calculated to be 8.9×10^{-5} emu gOe^{-1} and the magnetization of the NCs at 20 kOe is ∼1.8 emu g^{-1}, close to the value used for common bioseparation.[39]

In addition, for Eu^{3+}-doped KSc_2F_7 NCs, an enhancement of DC fluorescence intensity from the $^5D_0$–$^7F_2$ emission appears under 265 nm excitation after increasing the Eu^{3+} doping concentration (Fig. S10a†). What is more, 10% Eu^{3+}-doped NCs show a visible red color emission (Fig. S10b†).

4. Conclusions

In summary, a novel method to control the aspect ratio of the KSc_2F_7 NCs by lanthanide-doping was proposed. Doping KSc_2F_7 hosts with a RE^{3+} with a large ionic radius is beneficial for forming ultrasmall nanospheres, which can also be realized through increasing the doping concentration. Doping of a lanthanide with a larger ionic radius is equivalent to increasing the amount of the dopant on the aspect ratio evolution. These findings can act as an important tool for the controlled-synthesis of other analogous NCs, enabling customized designs of functional nanomaterials with desired morphology. Additionally, the lanthanide-doped KSc_2F_7 NCs also show favourable multifunctionality, such as multi-color UC emission, DC emission and magnetism. Therefore, they can be widely applied in the areas of display, solar energy, bioprobes, bioimaging, telecommunications, magnetic resonance imaging and so on.

Acknowledgements

The authors gratefully appreciate the support from the National Basic Research Program (2011CB933502) of China, and the National Natural Science Foundation (21335004, 21121091).

Notes and references

1 T. Cao, Y. Yang, Y. Sun, Y. Wu, Y. Gao, W. Feng and F. Li, *Biomaterials*, 2013, **34**, 7127.
2 R. Si, Y. W. Zhang, L. P. You and C. H. Yan, *Angew. Chem., Int. Ed.*, 2005, **44**, 3256.
3 J.-C. Boyer, L. A. Cuccia and J. A. Capobianco, *Nano Lett.*, 2007, **7**, 847.
4 H. Deng, S. Yang, S. Xiao, H.-M. Gong and Q.-Q. Wang, *J. Am. Chem. Soc.*, 2008, **130**, 2032.
5 J. Yang, D. Shen, X. Li, W. Li, Y. Fang, Y. Wei, C. Yao, B. Tu, F. Zhang and D. Zhao, *Chem.–Eur. J.*, 2012, **18**, 13642.
6 S. Zeng, J. Xiao, Q. Yang and J. Hao, *J. Mater. Chem.*, 2012, **22**, 9870.
7 D. Q. Chen and Y. S. Wang, *Nanoscale*, 2013, **5**, 4621.
8 X. Feng, D. C. Sayle, Z. L. Wang, M. S. Paras, B. Santora, A. C. Sutorik, T. X. T. Sayle, Y. Yang, Y. Ding, X. Wang and Y.-S. Her, *Science*, 2006, **312**, 1504.
9 F. Wang, Y. Han, C. S. Lim, Y. Lu, J. Wang, J. Xu, H. Chen, C. Zhang, M. Hong and X. Liu, *Nature*, 2010, **463**, 1061.
10 D. Chen, Y. Yu, F. Huang, P. Huang, A. Yang and Y. Wang, *J. Am. Chem. Soc.*, 2010, **132**, 9976.
11 Y. Yang, Y. Jin, H. He, Q. Wang, Y. Tu, H. Lu and Z. Ye, *J. Am. Chem. Soc.*, 2010, **132**, 13381.
12 J. He, I. D. Blum, H.-Q. Wang, S. N. Girard, J. Doak, L.-D. Zhao, J.-C. Zheng, G. Casillas, C. Wolverton, M. Jose-Yacaman, D. N. Seidman, M. G. Kanatzidis and V. P. Dravid, *Nano Lett.*, 2012, **12**, 5979.
13 I. López, E. Nogales, B. Méndez, J. Piqueras, A. Peche, J. Ramírez-Castellanos and J. M. González-Calbet, *J. Phys. Chem. C*, 2013, **117**, 3036.
14 J. He, L.-D. Zhao, J.-C. Zheng, J. W. Doak, H. Wu, H.-Q. Wang, Y. Lee, C. Wolverton, M. G. Kanatzidis and V. P. Dravid, *J. Am. Chem. Soc.*, 2013, **135**, 4624.
15 S. Huang, M. Bai and L. Y. Wang, *Sci. Rep.*, 2013, **3**, 2023.
16 M. An, J. Cui, Q. He and L. Wang, *J. Mater. Chem. B*, 2013, **1**, 1333.
17 H. Li and L. Wang, *Analyst*, 2013, **138**, 1589.
18 J. Zhao, D. Jin, E. P. Schartner, Y. Lu, Y. Liu, A. V. Zvyagin, L. Zhang, J. M. Dawes, P. Xi, J. A. Piper, E. M. Goldys and T. M. Monro, *Nat. Nanotechnol.*, 2013, **8**, 729.
19 S. J. Zeng, M. K. Tsang, C. F. Chan, K. L. Wong and J. H. Hao, *Biomaterials*, 2012, **33**, 9232.
20 X. Li, D. Shen, J. Yang, C. Yao, R. Che, F. Zhang and D. Zhao, *Chem. Mater.*, 2012, **25**, 106.
21 Y. Ding, H. Zhu, X. Zhang, J.-J. Zhu and C. Burda, *Chem. Commun.*, 2013, **49**, 7797.
22 Z. Gu, L. Yan, G. Tian, S. Li, Z. Chai and Y. Zhao, *Adv. Mater.*, 2013, **25**, 3758.
23 Y. Liu, D. Wang, J. Shi, Q. Peng and Y. Li, *Angew. Chem., Int. Ed.*, 2013, **52**, 4366.
24 N. Tu and L. Wang, *Chem. Commun.*, 2013, **49**, 6319.
25 F. Zhang, G. B. Braun, A. Pallaoro, Y. Zhang, Y. Shi, D. Cui, M. Moskovits, D. Zhao and G. D. Stucky, *Nano Lett.*, 2011, **12**, 61.
26 L. Y. Wang and Y. D. Li, *Chem. Mater.*, 2007, **19**, 727.
27 M. Deng, Y. Ma, S. Huang, G. Hu and L. Wang, *Nano Res.*, 2011, **4**, 685.
28 L. Wang and Y. Li, *Nano Lett.*, 2006, **6**, 1645.
29 Y. Ding, X. Teng, H. Zhu, L. Wang, W. Pei, J.-J. Zhu, L. Huang and W. Huang, *Nanoscale*, 2013, **5**, 11928.
30 X. Teng, Y. Zhu, W. Wei, S. Wang, J. Huang, R. Naccache, W. Hu, A. I. Y. Tok, Y. Han, Q. Zhang, Q. Fan, W. Huang, J. A. Capobianco and L. Huang, *J. Am. Chem. Soc.*, 2012, **134**, 8340.
31 S. Ye, Y.-j. Li, D.-c. Yu, G.-p. Dong and Q.-Y. Zhang, *J. Mater. Chem.*, 2011, **21**, 3735.
32 J. Yang, C. Zhang, C. Peng, C. Li, L. Wang, R. Chai and J. Lin, *Chem.–Eur. J.*, 2009, **15**, 4649.
33 Y. Su, B. Zhu, K. Guan, S. Gao, L. Lv, C. Du, L. Peng, L. Hou and X. Wang, *J. Phys. Chem. C*, 2012, **116**, 18508.

34 G. M. Dalpian and J. R. Chelikowsky, *Phys. Rev. Lett.*, 2006, **96**, 226802.
35 D. J. Norris, A. L. Efros and S. C. Erwin, *Science*, 2008, **319**, 1776.
36 T. Taniguchi, T. Watanabe, N. Sakamoto, N. Matsushita and M. Yoshimura, *Cryst. Growth Des.*, 2008, **8**, 3725.
37 G. K. Liu, H. Z. Zhuang and X. Y. Chen, *Nano Lett.*, 2002, **2**, 535.
38 S. Zeng, G. Ren, C. Xu and Q. Yang, *CrystEngComm*, 2011, **13**, 4276.
39 Z. Liu, G. Yi, H. Zhang, J. Ding, Y. Zhang and J. Xue, *Chem. Commun.*, 2008, 694.